

# Quantum phases of quadrupolar Fermi gases in optical lattices

S. G. Bhongale,<sup>1</sup> Ludwig Mathey,<sup>2</sup> Erhai Zhao,<sup>1</sup> Susanne F. Yelin,<sup>3,4,5</sup> and Mikhail Lemeshko<sup>4,5,\*</sup>

<sup>1</sup>*School of Physics, Astronomy, and Computational Sciences, George Mason University, Fairfax, VA 22030*

<sup>2</sup>*Zentrum für Optische Quantentechnologien and Institut für Laserphysik, Universität Hamburg, 22761 Hamburg, Germany*

<sup>3</sup>*Department of Physics, University of Connecticut, Storrs, Connecticut 06269*

<sup>4</sup>*ITAMP, Harvard-Smithsonian Center for Astrophysics, 60 Garden Street, Cambridge, MA 02138*

<sup>5</sup>*Department of Physics, Harvard University, 17 Oxford Street, Cambridge, MA 02138*

(Dated: October 18, 2018)

We introduce a new platform for quantum simulation of many-body systems based on nonspherical atoms or molecules with zero dipole moment but possessing a significant value of electric quadrupole moment. We consider a quadrupolar Fermi gas trapped in a 2D square optical lattice, and show that the peculiar symmetry and broad tunability of the quadrupole-quadrupole interaction results in a rich phase diagram encompassing unconventional BCS and charge density wave phases, and opens up a perspective to create topological superfluid. Quadrupolar species, such as metastable alkaline-earth atoms and homonuclear molecules, are stable against chemical reactions and collapse and are readily available in experiment at high densities.

PACS numbers: 67.85.-d, 75.30.Fv, 71.10.Fd

Quantum gases of ultracold atoms have provided a fresh perspective on strongly-correlated many-body states, by establishing a highly tunable environment in which both open questions of solid state physics and novel, previously unobserved, many-body states can be studied [1]. An important landmark was reached by cooling and trapping dipolar atoms and molecules, bosonic and fermionic [2–7], near or into quantum degeneracy, which extended the range of features available to quantum simulation in ultracold atom systems beyond contact interactions. Numerous exotic states such as supersolids, quantum liquid crystals and bond-order solids have been predicted, extended Hubbard models with 3-body interactions, and highly tunable lattice spin models for quantum magnetism have been proposed [8–13]. The crucial feature of the interactions in dipolar gases is their anisotropic and long-range character tunable with static and radiative fields [13–15], which is key to the intriguing many-body effects that have been predicted.

In this Letter we propose to study quadrupolar quantum gases. This constitutes a new class of systems in ultracold physics, which can be used as a platform for quantum simulation. Quadrupole interactions are most visible for non-polar particles which possess a significant electric quadrupole moment. The angular dependence of the resulting quadrupole-quadrupole interaction is substantially different compared to the dipole-dipole one, due to the higher-order symmetry. For atoms or molecules in an optical lattice, this allows for broad tunability of the nearest and next-nearest neighbor couplings. As a concrete example, we discuss metastable alkaline-earth atoms and homonuclear molecules which have comparatively large quadrupolar moments. In order to demonstrate rich many-body effects that arise in ensembles of such particles, we derive the quantum phase diagram of a quadrupolar fermionic gas in an optical lattice at

half-filling. We find that several unconventional phases emerge, such as bond order solids and  $p$ -wave pairing, and discover the intriguing possibility of creating topological ground states of  $p_x + ip_y$  symmetry. While dipolar quantum gases were also shown to host novel many-body phases, quadrupolar particles are available in experiment at higher densities and are stable against chemical reactions [16] and collapse [17].

In order to determine the quadrupole-quadrupole interaction energy, we consider the potential of a classical quadrupole with moment  $q = \int \rho(\vec{r})r^2(3\cos^2\theta - 1)d\vec{r}$  located at  $\vec{r}_0 = 0$  aligned in  $\hat{k}$ -direction. Here  $\rho(\vec{r})$  is the electron charge density and  $\cos\theta \equiv \hat{k} \cdot \hat{r}$  [47]. In this work we focus on systems possessing cylindrical symmetry, for which only one component  $q$  of the quadrupole moment tensor  $q_{ij}$  is nonzero. The electric field potential generated by the quadrupole is given by  $\phi(\vec{r}) = \frac{q}{4r^3}(3\cos^2\theta - 1)$ . If a second quadrupole with the same alignment  $\hat{k}$  is placed at location  $\vec{r}$ , the resulting interaction energy is

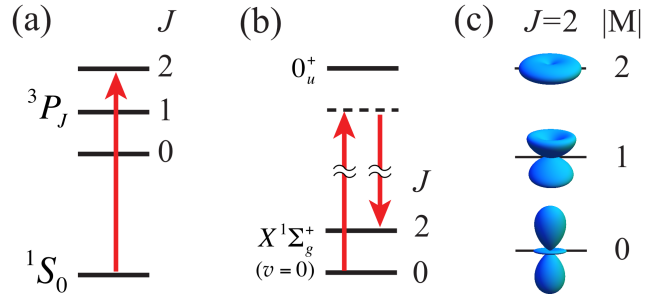


FIG. 1: Recipe for realization of quadrupolar particles: (a) with alkaline-earth atoms in long-living  $^3P_2$  levels; and (b) with homonuclear molecules in rotational states with  $J > 0$ . (c) Angular “shape” of quadrupolar particles exemplified by  $|2, M\rangle$  states.

$V_{cl}^{qq} = \frac{q}{4}(\hat{k} \cdot \nabla)(\hat{k} \cdot \nabla\phi) = \frac{3q^2}{16r^5}(35\cos^4\theta - 30\cos^2\theta + 3)$ . While the functional form of this potential carries over to the quantum description, the prefactor of the interaction for two states has to be obtained via a quantum definition of the quadrupole moment  $\mathbf{q}_2$ . The latter is a spherical tensor of rank two with components defined in atomic units as  $q_{2,M} = -\sum_k r_k^2 C_{2,M}(\theta_k, \phi_k)$ , where  $(r_k, \theta_k, \phi_k)$  give the coordinates of the  $k$ -th electron of the particle, and  $C_{2,M}(\theta_k, \phi_k) = \sqrt{4\pi/5} Y_{2,M}(\theta_k, \phi_k)$  are the reduced spherical harmonics [18]. In the angular momentum basis,  $|J, M\rangle$ , with  $M$  being the projection of the angular momentum,  $\mathbf{J}$ , onto the quantization axis, the quadrupole operator couples the states with  $\Delta J = 0, \pm 2$ , so to first order any state with  $J > 1/2$  possesses a nonzero quadrupole moment [48]. Thus the value of the quadrupole moment can be controlled by preparing the particles in a particular  $|J, M\rangle$ -state, or their combination, using optical or microwave fields. The quadrupole interaction reads

$$V^{qq} = \frac{\sqrt{70}}{r^5} \sum_{\alpha} (-1)^{\alpha} C_{4,-\alpha}(\theta, \phi) [\mathbf{q}_2^{(1)} \otimes \mathbf{q}_2^{(2)}]_{4,\alpha}, \quad (1)$$

where  $(r, \theta, \phi)$  gives the vector between particles, and  $[\mathbf{q}_2^{(1)} \otimes \mathbf{q}_2^{(2)}]_{4,\alpha}$  is a spherical tensor of rank four formed from two quadrupole moments. For both particles prepared in the same  $|J, M\rangle$  state, Eq. (1) reduces to  $V^{qq} = V(3 - 30\cos^2\theta + 35\cos^4\theta)/r^5$ , with  $V = q^2 3(J^2 + J - 3M^2)^2 / [4(4J^2 + 4J - 3)^2]$ , where  $q = 2\langle 2, 2 | q_{2,0} | 2, 2 \rangle$ , which coincides with the classical definition [19]. We note that in the classical limit of  $J \rightarrow \infty$ , and for  $M = J$ , the prefactor  $V = 3q^2/16$  of the classical expression is recovered. The interaction can then be attractive or repulsive depending on the angle  $\theta$ .

Among the particles for which the quadrupolar moment is known, the most promising candidates for the experimental realization of quadrupolar quantum gases are metastable alkaline-earth atoms [19–23] and homonuclear diatomic molecules [24, 25]. Alkaline-earth atoms, such as Sr, and some of the rare-earth atoms, such as Yb, can be prepared in metastable  $^3P_2^o$  states, whose lifetime exceeds thousands of seconds [19–23, 26], by optical excitation, cf. Fig. 1 (a). Both bosonic and fermionic isotopes of Sr and Yb have been brought to quantum degeneracy [27–30]. Ultracold homonuclear molecules, such as Cs<sub>2</sub> or Sr<sub>2</sub>, can be prepared in the absolute ground state,  $^1\Sigma_g^+(v=0, J=0)$ , and then transferred to a rotational state with  $J > 0$ , using a Raman transition [24, 25, 31], cf. Fig. 1 (b). While homonuclear molecules are always bosons, fermionic quadrupolar molecules can be prepared using distinct isotopes of the same species [32]. For both atoms and molecules the degeneracy of a particular  $J$  level can be lifted by an external electric or magnetic field,  $\mathbf{F}$ . We consider the regime when the quadrupole-quadrupole interactions dominate the behavior of the system, i.e. the electric field  $\mathbf{F}$  is too weak to induce a sub-

stantial value of a dipole moment, or the particles are prepared in a non-magnetic Zeeman component. The typical “shapes” of quadrupolar states are exemplified in Fig. 1 (c). Both atoms and molecules can be prepared in the  $|2, 0\rangle$  ( $|2, 2\rangle$ ) states using two linearly (circularly) polarized photons; the quadrupole-quadrupole interaction is equal in these cases and is larger than for the  $|2, 1\rangle$  states.

The quadrupole moments for metastable alkaline-earth atoms and homonuclear molecules are similarly on the order of 10–40 a.u. [19–23, 25], which gives an interaction strength,  $V^{qq}$ , on the order of a few Hz at 266 nm lattice spacing. Furthermore, interactions on the order of 1 kHz can be achieved for 100 nm lattice spacings realizable with atoms trapped in nanoplasmonic structures [33]. We note that the dispersion (van der Waals) interaction,  $V^{\text{dis}} \sim r^{-6}$ , is  $10^2 - 10^3$  times smaller at typical optical lattice spacings [21], therefore the quadrupole-quadrupole interaction dominates the physics of these systems. Quantum gases can be trapped for tens of seconds, so the observation of many-body phases generated by these interactions is feasible via the standard techniques, ranging from time-of-flight detection to noise correlation and Bragg spectroscopy.

To illustrate the intriguing many-body effects that can arise in these systems, we investigate the quantum phase diagram of a system of interacting quadrupolar fermions on a square lattice, at half-filling. We assume every particle to be prepared in state  $|J, M\rangle$ , where  $\mathbf{J}$  is the electronic (for atoms) or rotational (for molecules) angular momentum, and  $M$  is the projection of  $\mathbf{J}$  on the direction  $\hat{F} = (\theta_F, \phi_F)$  in the laboratory frame given by the external field  $\mathbf{F}$  used to lift the  $M$ -degeneracy. The particles are confined to a lattice with a lattice constant  $a_L$ , corresponding to the Hamiltonian:

$$H = -t \sum_{\langle i,j \rangle} c_i^\dagger c_j + \frac{1}{2} \sum_{i \neq j} V_{ij} c_i^\dagger c_i c_j^\dagger c_j, \quad (2)$$

where  $t$  represents the nearest-neighbor hopping and  $c_i$  is the fermion annihilation operator at the  $i$ -th lattice site. Throughout the remainder of the paper, we use  $a_L$  as a unit of length and  $t$  as a unit of energy. As schematically shown in Fig. 2 (a), the interaction strength  $V_{ij}$  depends on the orientation of the vector connecting the quadrupoles,  $\mathbf{r} = \mathbf{r}_i - \mathbf{r}_j$ , relative to the field direction,  $\hat{F}$ , via  $V_{\mathbf{r}} \equiv V_{ij} = \langle ij | V^{qq} | ij \rangle = V[3 - 30(\hat{r} \cdot \hat{F})^2 + 35(\hat{r} \cdot \hat{F})^4]/r^5$ . Thus, one can immediately observe that the interaction between two quadrupoles can be tuned either attractive or repulsive, by changing the orientation of the external field  $\mathbf{F}$ . Fig. 2 (b) shows the  $(\theta_F, \phi_F)$ -dependence of the interaction matrix element between the nearest- and next-nearest neighbors. The richness of the quadrupolar interaction becomes apparent in this figure. There are several regions in which the signs and the relative magnitudes of  $\{V_{\mathbf{r}}\}$ ,

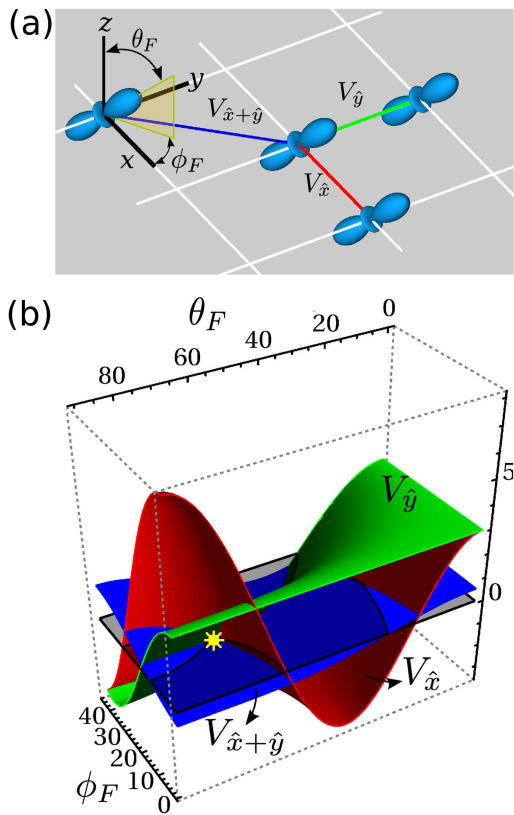


FIG. 2: (a) Schematic representation of quadrupolar fermions on a square lattice. Alignment of the quadrupoles is given by the quantization axis of the external field  $\mathbf{F}$ , pointing along  $\hat{F} = (\theta_F, \phi_F)$ . The nearest-neighbor interaction is represented by green and red solid lines, while the next-nearest neighbor interaction is shown in blue. (b) 3D plot showing the interactions  $V_{\hat{x}}$  (red),  $V_{\hat{y}}$  (green), and  $V_{\hat{x}+\hat{y}}$  (blue) as a function of the angles  $(\theta_F, \phi_F)$ ; “\*” marks the point in the vicinity of which both  $V_{\hat{x},\hat{y}}$  and  $V_{\hat{x}+\hat{y}}$  change the sign.

$V_{\hat{y}}, V_{\hat{x}+\hat{y}}$  show distinctive characteristics. For example, in the region  $(\theta_F \lesssim 25^\circ, 0^\circ \leq \phi_F \leq 45^\circ)$ , both nearest- and next-nearest neighbor interactions are repulsive, while they all become attractive in the region  $(30^\circ \lesssim \theta_F \lesssim 60^\circ, \phi_F \sim 45^\circ)$ . Furthermore, one can identify finite regions where either one or two of  $\{V_{\hat{x}}, V_{\hat{y}}, V_{\hat{x}+\hat{y}}\}$  is attractive while the rest is repulsive.

Interactions of opposite sign can result in competition between quantum phases of different symmetry, resulting in frustration. Thus, fermions with dominant quadrupolar interactions provide an interesting setup for studying many-body physics with competing phases. For example, in the vicinity of  $(90^\circ, 45^\circ)$  both  $V_{\hat{x}}$  and  $V_{\hat{y}}$  are attractive, while  $V_{\hat{x}+\hat{y}}$  is repulsive (see Fig. 2). On general grounds, one would expect a BCS type ground state resulting from condensation of Cooper pairs due to the attractive  $V_{\hat{x}}$  and  $V_{\hat{y}}$  couplings. However, the repulsive  $V_{\hat{x}+\hat{y}}$  interaction, if significant, may lead to the insurgence of some other phase, and therefore needs to be

quantitatively accounted for. As another intriguing example, in the vicinity of  $(40^\circ, 5^\circ)$ ,  $V_{\hat{x}}$  is strongly attractive while  $V_{\hat{y}}$  is strongly repulsive. As we show below, the ground state in this region is neither a BCS state nor conventional charge density wave (CDW). These two examples show that the actual ground state may be of an unexpected nature. Exposing the true ground state thus demands a theory that is (i) unbiased with respect to the initial ansatz, and (ii) includes fluctuations.

Issue (ii) can be adequately addressed within the renormalization group (RG) analysis at weak couplings, where the low energy physics near the Fermi surface is extracted by successively integrating out the high energy degrees of freedom [34]. In order to satisfy criterion (i), we employ the exact (or “functional”) renormalization group (FRG) which keeps track of all the interaction vertices, including both the particle-particle and particle-hole channels, and treats all instabilities on equal footing [35][49].

The FRG phase diagram, Fig. 3 (a), features several different kinds of BCS and CDW phases with symmetry indicated by the the polar plots of Fig. 3 (b).  $CDW_s$  is a CDW phase with a checkerboard modulation of on-site densities, occurring in regions where the repulsive interaction between nearest neighbors dominates, see Fig. 2. This happens for all values of  $\phi_F$  when  $\theta_F \lesssim 25^\circ$ , and also for  $\phi_F \lesssim 22^\circ$  at large  $\theta_F \gtrsim 60^\circ$ . In addition, two novel types,  $CDW_{p_x}$  and  $CDW_{p_y}$ , are present. They correspond to a checkerboard modulation of the effective hopping between nearest neighbors along the  $x$  and  $y$  direction respectively, i.e.,  $\langle c_i^\dagger c_j \rangle$  with  $\mathbf{r}_i - \mathbf{r}_j = \hat{x}$  or  $\hat{y}$ , with the average taken over the many-body ground state. We refer to these phases as to bond order solids (BOS). In comparison, the  $s$ -wave CDW order corresponds to modulations of  $\langle c_i^\dagger c_i \rangle$ . Furthermore, we find a small region of  $CDW_{s+d}$  that involves a mixture of extended  $s$ - and  $d$ -waves. Together they give rise to a checkerboard modulation of effective hopping between the next-nearest neighbor sites. The  $CDW_{p_x}$ ,  $CDW_{p_y}$ , and  $CDW_{s+d}$  can be thought of as a 2D generalization of the bond-order-wave phase occurring in the extended Hubbard model in one dimension [36–38]. While BOS is expected for dipolar fermions in 2D [12], it occupies a significantly larger region of the parameter space for quadrupolar interactions (e.g., it is stabilized as soon as  $\theta_F$  approaches  $25^\circ$ ). Moreover, the angular dependence of quadrupolar interactions is substantially more complex, resulting in two BOS phases of  $p_y$  and  $p_x$  symmetries, appearing at small and large  $\theta_F$ , respectively. Interestingly, these two phases occur in the regions where  $V_{\hat{x}}$  and  $V_{\hat{y}}$  are comparable in magnitude but opposite in sign, i.e.,  $CDW_{p_x(p_y)}$  is stabilized when  $V_{\hat{x}(\hat{y})}$  is repulsive while  $V_{\hat{y}(\hat{x})}$  is attractive, cf. Fig. 2 (b). Thus, quadrupolar Fermi gases are well suited for exploring the properties of nonzero angular momentum (i.e. unconventional) density wave phases.

Finally there are two BCS phases, which mostly occur where both  $V_{\hat{x}}$  and  $V_{\hat{y}}$  are attractive. Our FRG analy-

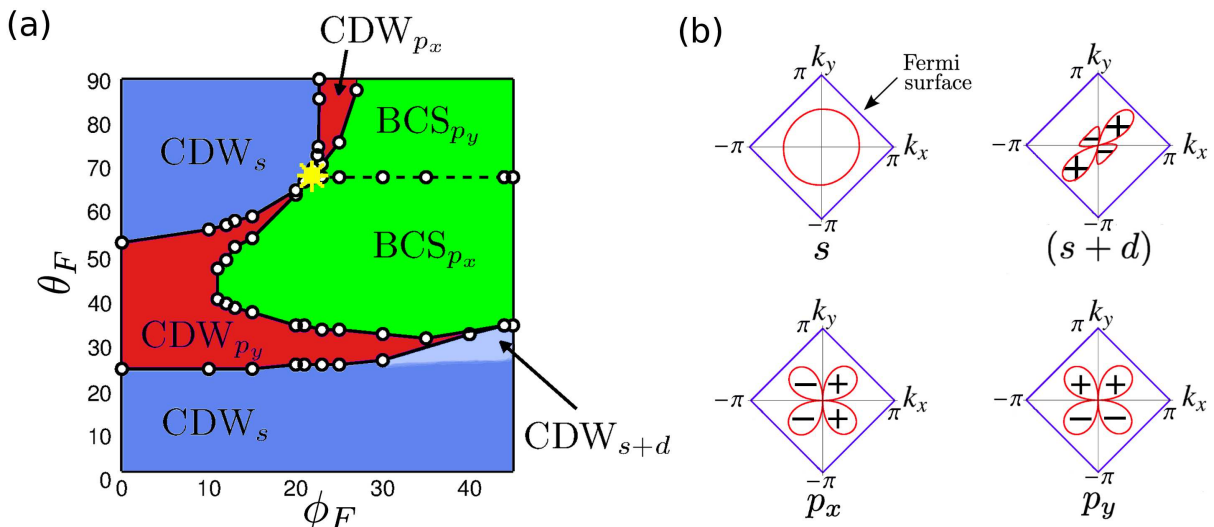


FIG. 3: Quantum phase diagram for quadrupolar fermions on a square lattice. (a) FRG phase diagram in the weak coupling limit,  $V/t = 0.2$ , and at half filling shown as a function of the magnetic field direction  $\hat{F} = (\theta_F, \phi_F)$ . The point marked by “\*”, where 5 different phases seem to meet, corresponds to  $V_{\hat{x}}, V_{\hat{y}}, V_{\hat{x}+\hat{y}} \approx 0$  as shown in Fig. 2 (b). This suggests the likelihood of almost three distinct tri-critical points in close proximity to each other, which are hard to resolve due to the smallness of the couplings. (b) The orbital symmetry of the CDW and BCS phases shown in (a) is plotted in red. This symmetry corresponds to the symmetry of the most divergent eigenvector of the BCS and CDW vertices combined. The  $p_x$  ( $p_y$ ) wave CDW has the same orbital structure as the  $p_x$  ( $p_y$ ) wave BCS.

sis shows that the BCS phase can be stable even though the next-nearest neighbor interaction is weakly repulsive. We find that the symmetry of the BCS order parameter is  $p_x$  or  $p_y$ , depending on whether  $V_{\hat{x}}$  or  $V_{\hat{y}}$  is more attractive. Along the line of  $\theta_F \sim 65^\circ$  these two BCS phases are degenerate. This raises the possibility of realizing  $p_x + ip_y$  topological superfluid order. By analogy with the proposal of Ref. [39], using an AC field to periodically modulate the direction of  $(\theta_F, \phi_F)$ , one can lift the degeneracy and engineer the chiral  $p_x + ip_y$  state.

In conclusion, we have shown that ultracold Fermi gases with quadrupole-quadrupole interactions can be used to study unconventional BCS, CDW, and topological phases, and gain insight into the physics of competing ground states. While we have focused on the specific case of a square lattice at half-filling, the functional RG methods of this work can be applied to study other fillings and lattice geometries. Temperatures achieved for degenerate Fermi gases of alkaline-earth atoms in experiment are  $T = 0.26 T_F$  and  $T = 0.37 T_F$  respectively [29, 30]. The optimal  $T_c$  for the CDW and BCS phases predicted here is estimated to be on the order of  $0.03 T_F$ , for intermediate couplings,  $V \sim t$ . Thus these many-body phases seem to be within experimental reach in the near future.

Since quadrupolar interactions occur in numerous subfields of physics, from molecular photofragmentation [40] and structure of  $f$ -electron compounds [41] to nuclear reactions [42] and gravitation of black holes [43], the proposed quantum simulation platform can in principle be applied beyond the many-body physics of fermionic

gases. Finally, we note that ground-state atoms can be provided with significant quadrupole moments by means of Rydberg dressing, i.e. admixing a highly-excited electronic state possessing a large quadrupole moment with far-detuned laser light [44, 45].

We are grateful to Charles Clark, Robin Coté, Hendrik Weimer, and Shan-Wen Tsai for discussions. S.B. and E.Z. are supported by NSF (PHY-1205504) and NIST (60NANB12D244). L.M. acknowledges support from the Landesexzellenzinitiative Hamburg, which is financed by the Science and Research Foundation Hamburg and supported by the Joachim Herz Stiftung, and from the Deutsche Forschungsgemeinschaft under SFB 925. M.L. acknowledges support from NSF through a grant for the Institute for Theoretical Atomic, Molecular, and Optical Physics at Harvard University and Smithsonian Astrophysical Observatory. S. F. Y. acknowledges financial support from the National Science Foundation and Air Force Office of Scientific Research.

## SUPPLEMENTAL MATERIAL

### Functional Renormalization Group

Renormalization group (RG) is a symmetry transformation allowing to map the Hamiltonians or actions defined in a certain phase space to those in the same phase space. If one represents the initial action as a point in the coupling constant space, this point will move under the RG transformation to another point in the same space, implying a *flowing* coupling constant as the RG transformation is performed repeatedly. This automatically gives rise to the notion of a fixed point where the flow stops implying constancy of couplings under the RG transformation. Furthermore, the RG transformation, associated with a finite cutoff, allows for separation between the modes of interest (low energy degrees of freedom) and the rest, by decreasing the cutoff accompanied by a suitable change in couplings such that the theory is invariant.

The ground state of a non-interacting Fermi system is a filled Fermi sea bounded by the Fermi surface (FS). Such a non-interacting ground state has gapless excitations corresponding to promoting a fermion from just below the FS to above the FS. However, if some perturbation is added to the free system, will the system develop a gap or remain gapless? This connection,  $T = 0$  *gapless* Fermi liquid as a RG fixed point, and the various *gapped* quantum phases as Fermi surface instabilities associated with diverging RG flow, was originally introduced by Shankar [34]. The method used here, the functional renormalization group (FRG), is a generalization of Shankar's renormalization-group to an arbitrary Fermi surface [34]. The Kadanoff-Wilson mode elimination (developed by Shankar for 2D fermions) applied to the effective action with only two particle interaction retains only strictly logarithmic contributions to the flow. Therefore, *e.g.*, even if the nesting is good but not perfect, the corresponding singularity in the  $p-h$  channel is destroyed reducing the RG-flow to zero. As one can imagine, this could be a serious issue when analyzing situations where the low energy physics is an outcome of the interplay between several competing channels. As a remedy, Zanchi and Schulz derived the functional renormalization group technique [35] as a generalization of the Kadanoff-Wilson-Polchinski group [46] that was originally formulated in the context of quantum fields with one single zero energy point in momentum space.

The starting point of the renormalization group for a many-fermion model Hamiltonian is the partition function given by

$$\mathcal{Z} = \int \sum_{\gamma, \sigma} \mathcal{D}\bar{\psi}_{\gamma, \sigma} \mathcal{D}\psi_{\gamma, \sigma} e^{S[\bar{\psi}_{\gamma, \sigma}, \psi_{\gamma, \sigma}]}$$

where the integration is carried out over Grassmann variables  $\{\bar{\psi}_{\gamma, \sigma}, \psi_{\gamma, \sigma}\}$  for all fermions in the Brillouin zone

where the index  $\gamma$  represents energy-momentum vector  $(\omega_n, \mathbf{k})$  and  $\sigma$  is the spin. Since we are interested in the low energy physics, the goal is to find an effective action that depends only on the low energy degrees of freedom close to the Fermi surface. If we assume that the slow modes, as illustrated in supplementary figure 4, are in a shell  $\pm\Lambda$  about the Fermi surface, then the action  $S$  maybe decomposed as

$$S\{\psi\} = S_0\{\psi_{<}\} + S_0\{\psi_{>}\} + S_I\{\psi_{<}, \psi_{>}\},$$

where  $S_0$  is the non-interacting piece and  $S_I$  comes from the two-particle interaction. Now, from the definition of the partition function, it is easy to see that the low energy effective action can be formally written as a partial trace over the high energy degrees of freedom as:

$$S_\Lambda\{\psi_{<}\} = \ln \int \mathcal{D}\bar{\psi}_{>} \mathcal{D}\psi_{>} e^{S\{\psi_{<}, \psi_{>}\}}$$

Further, this effective action can always be decomposed into three terms,

$$S_\Lambda\{\psi_{<}\} = S\{\psi_{<}\} + \Omega_{>} + \delta S\{\psi_{<}\}$$

Here  $\Omega_{>}$  is the grand potential (times  $\beta$ ) of the fast fermions as if they were decoupled from the slow ones, and  $\delta S_{<}$  is the correction arising from coupling to the fast ones. This correction essentially gives rise to terms that are quadratic, quartic, etc, in field variables, thus renormalizing the corresponding self energy, two-point vertex, etc, respectively. Now all that remains is to rescale the momenta and field variables so that that  $S_\Lambda$  describes the low energy physics over the same kinematic range as before, allowing the proper comparison of the old and new couplings.

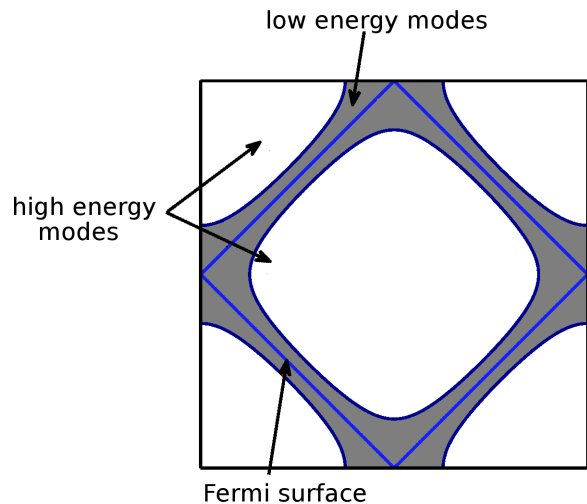


FIG. 4: Schematic indicating the low energy modes in the vicinity of the Fermi surface for 2D fermions on square lattice.

However, the problem that remains to be addressed is to decide at what order the effective action can be truncated so that the relevant low energy physics is captured. For fermions near the Fermi surface, even if the bare couplings are small, some of the diagrams, for example the particle-hole bubble, can acquire large values depending on the shape of the Fermi surface. Thus, in principle all  $p-h$  diagrams will have to be summed over. Such a sum (one example is the random phase approximation (RPA)) can only be controllably carried out in a limited number of situations and even those are rendered inefficient if the couplings are large.

The FRG provides a tractable way of book keeping the order of diagrams by defining an infinitesimal group

transformation

$$S \equiv S_{\Lambda_0} \rightarrow S'_{\Lambda_0 e^{-\ell}}$$

where  $\Lambda_0$  is the initial cutoff and  $\Lambda = \Lambda_0 e^{-\ell}$ . Thus at each step  $\Lambda d\ell$  modes are eliminated at a shell size  $\Lambda$ . In terms of diagrams this procedure allows for classification of diagrams in order of  $d\ell$ . However, since every internal line is constrained to a shell, a diagram of order  $(d\ell)^m$  will have  $m$  internal lines. Now, since  $d\Lambda$  is infinitesimal, only diagrams with one internal line dominates at every step of RG. This allows for grouping diagrams with equal number of external legs, resulting in the following Polchinski equation (flow equation) for the vertex  $\Gamma_{2n}^\ell$

$$\begin{aligned} \frac{\partial}{\partial \Lambda_\ell} \Gamma_{2n}^{(\ell)}(K_1, K_2, \dots, K_{2n}) &= \sum_{I_1, I_2} T \sum_{\omega_n} \int_{d\Lambda} d^2 k \Gamma_{2p}^{(\ell)}(-K, I_1) G_\ell(K) \Gamma_{2q}^{(\ell)}(K, I_2) \\ &\quad - T \sum_{\omega_n} \int_{d\Lambda} d^2 k \Gamma_{2(n+1)}^{(\ell)}(K, K_1, \dots, K_n, K, K_{n+1}, \dots, K_{2n}) G_\ell(K), \end{aligned}$$

where  $I_1 \cup I_2 = \{K_1, K_2, \dots, K_{2n}\}$  and the propagator is defined at each step by

$$G_\ell(K) = \left[ \Gamma_2^{(\ell)}(K) \right]^{-1}$$

The possible vertex diagrams with  $2n$  external lines and one internal line are shown in Supplementary Figure 5.

### Numerical Implementation

The Fermi surface (FS) of the non-interacting system of quadrupoles on a square lattice is a nested square at half filling. We discretize the FS into  $N = 32$  patches with momenta  $\mathbf{k}_i$ ,  $i \in \{1, 2, \dots, N\}$ . The 4-point interaction vertex as a function of three momenta  $\Gamma_4^{(\ell)}(\mathbf{k}_1, \mathbf{k}_2, \mathbf{k}_3) \equiv U_\ell(\mathbf{k}_1, \mathbf{k}_2, \mathbf{k}_3)$  is represented as a  $N^3 \times N^3$  matrix. We start with the bare vertices defined on the discretized Fermi surface,  $U_{\ell=0}(\mathbf{k}_i, \mathbf{k}_j, \mathbf{k}_l) = V_{\mathbf{k}_i - \mathbf{k}_l}$ , where  $V_{\mathbf{q}}$  is the quadrupole interaction in momentum space, i.e., the lattice Fourier transform of  $V_{\mathbf{r}}$  given in the main text, with proper anti-symmetrization required by Fermi statistics. The momentum dependence of the interaction is fully taken into account. At each FRG step  $\ell$ , the renormalized vertices  $U_\ell(\mathbf{k}_i, \mathbf{k}_j, \mathbf{k}_l)$  are calculated at one-loop level, truncating the effective action at the six fermion terms and neglecting self-energy correction [35]. The renormalized vertices for particular channels, e.g.  $U_\ell^{\text{CDW}}(\mathbf{k}_1, \mathbf{k}_2) \equiv U_\ell(\mathbf{k}_1, \mathbf{k}_2, \mathbf{k}_1 + \mathbf{Q})$  and  $U_\ell^{\text{BCS}}(\mathbf{k}_1, \mathbf{k}_2) \equiv U_\ell(\mathbf{k}_1, -\mathbf{k}_1, \mathbf{k}_2)$ , are then extracted by

appropriately choosing the in-coming and out-going momenta and  $\mathbf{Q} = (\pm\pi, \pm\pi)$  is the nesting vector. The channel with the most divergent eigenvalue represents the dominant instability of the FS, thereby indicating the nature and symmetry of incipient order parameter.

\* Electronic address: mlemeshko@cfa.harvard.edu

- [1] I. Bloch, J. Dalibard, and W. Zwerger, *Rev. Mod. Phys.* **80**, 885 (2008).
- [2] K. K. Ni, S. Ospelkaus, M. H. G. de Miranda, A. Pe'er, B. Neyenhuis, J. J. Zirbel, S. Kotochigova, P. S. Julienne, D. S. Jin, and J. Ye, *Science* **322**, 231 (2008).
- [3] A. Chotia *et al.*, *Phys. Rev. Lett.* **108**, 080405 (2012).
- [4] J. Deiglmayr, A. Grochola, M. Repp, K. Mörzlbauer, C. Glück, J. Lange, O. Dulieu, R. Wester, and M. Weidemüller, *Physical Review Letters* **101**, 133004 (2008).
- [5] A. Griesmaier, J. Werner, S. Hensler, J. Stuhler, and T. Pfau, *Phys. Rev. Lett.* **94**, 160401 (2005).
- [6] M. Lu, N. Q. Burdick, and B. L. Lev, *Phys. Rev. Lett.* **108**, 215301 (2012).
- [7] K. Aikawa, A. Frisch, M. Mark, S. Baier, A. Rietzler, R. Grimm, and F. Ferlaino, *Phys. Rev. Lett.* **108**, 210401 (2012).
- [8] M. A. Baranov, *Physics Reports* **464**, 71 (2008).
- [9] T. Lahaye, C. Menotti, L. Santos, M. Lewenstein, and T. Pfau, *Rep. Prog. Phys.* **72**, 126401 (2009).
- [10] B. Capogrosso-Sansone *et al.*, *Phys. Rev. Lett.* **104**, 125301 (2010).
- [11] B. M. Fregoso and E. Fradkin, *Phys. Rev. Lett.* **103**, 205301 (2009).
- [12] S. G. Bhongale, L. Mathey, S. W. Tsai, C. W. Clark, and

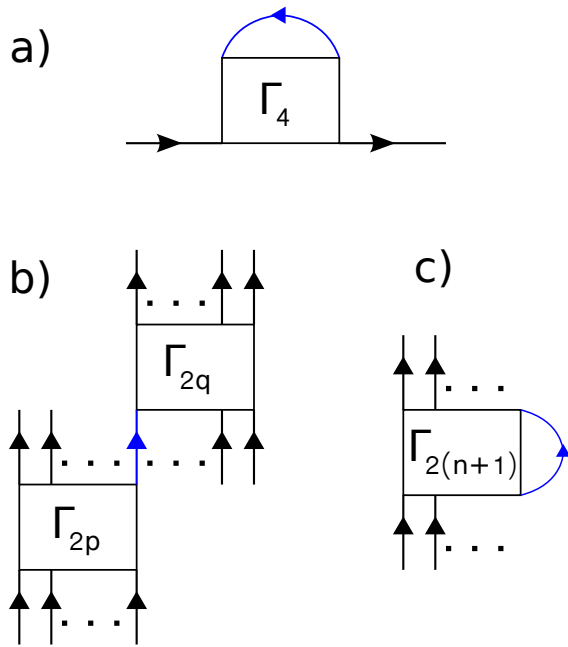


FIG. 5: Possible vertex diagrams with one internal line (shown in blue), that is integrated over the shell  $\Lambda$ . a)  $\Gamma_{2n}$  for  $n = 2$ , b) and c) correspond to possible vertex diagrams for  $n > 2$ .

- E. Zhao, Phys. Rev. Lett. **108**, 145301 (2012).
- [13] A. V. Gorshkov, S. R. Manmana, G. Chen, E. Demler, M. D. Lukin, and A. M. Rey, Phys. Rev. A **84**, 033619 (2011).
- [14] M. Lemeshko, Phys. Rev. A **83**, 051402(R) (2011).
- [15] M. Lemeshko, R. V. Krems, and H. Weimer, Phys. Rev. Lett. **109**, 035301 (2012).
- [16] S. Ospelkaus, K.-K. Ni, D. Wang, M. H. G. de Miranda, B. Neyenhuis, G. Quémener, P. S. Julienne, J. L. Bohn, D. S. Jin, and J. Ye, Science **327**, 853 (2010).
- [17] T. Koch, T. Lahaye, J. Metz, B. Fröhlich, A. Griesmaier, and T. Pfau, Nat. Phys. **4**, 218 (2008).
- [18] D. A. Varshalovich, A. N. Moskalev, and V. K. Khersonski, *Quantum theory of angular momentum* (World Scientific Publications, Singapore and Teaneck, N.J., 1988).
- [19] A. Derevianko, Phys. Rev. Lett. **87**, 023002 (2001).
- [20] B. B. Jensen, H. Ming, P. G. Westergaard, K. Gunnarsson, M. H. Madsen, A. Bruschi, J. Hald, and J. W. Thomsen, Phys. Rev. Lett. **107**, 113001 (2011).
- [21] R. Santra, K. Christ, and C. Greene, Phys. Rev. A **69**, 042510 (2004).
- [22] R. Santra and C. H. Greene, Phys. Rev. A **67**, 062713 (2003).
- [23] A. A. Buchachenko, Eur. Phys. J. D **61**, 291 (2011).
- [24] R. V. Krems, W. C. Stwalley, and B. Friedrich, eds., *Cold molecules: theory, experiment, applications* (Taylor&Francis/CRC, Boca Raton, FL, 2009).
- [25] J. N. Byrd, R. Côté, and J. A. Montgomery, Journal of Chemical Physics **135**, 244307 (2011).
- [26] S. B. Nagel, C. E. Simien, S. Laha, P. Gupta, V. S. Ashoka, and T. C. Killian, Phys. Rev. A **67**, 011401(R) (2003).
- [27] T. Fukuhara, S. Sugawa, and Y. Takahashi, Phys. Rev. A **76**, 051604 (2007).
- [28] S. Stellmer, M. K. Tey, B. Huang, R. Grimm, and F. Schreck, Phys. Rev. Lett. **103**, 200401 (2009).
- [29] B. DeSalvo, M. Yan, P. Mickelson, Y. Martinez de Escobar, and T. Killian, Phys. Rev. Lett. **105**, 030402 (2010).
- [30] T. Fukuhara, Y. Takasu, M. Kumakura, and Y. Takahashi, Phys. Rev. Lett. **98**, 030401 (2007).
- [31] I. Manai, R. Horchani, H. Lignier, P. Pillet, D. Comparat, A. Fioretti, and M. Allegrini, Phys. Rev. Lett. **109**, 183001 (2012).
- [32] S. B. Papp and C. E. Wieman, Phys. Rev. Lett. (2006).
- [33] M. Gullans, T. Tiecke, D. E. Chang, J. Feist, J. D. Thompson, J. I. Cirac, P. Zoller, and M. D. L. 1, arXiv:1208.6293 (2012).
- [34] R. Shankar, Rev. Mod. Phys. **66**, 129 (1994).
- [35] D. Zanchi and H. J. Schulz, Phys. Rev. B **61**, 13609 (2000).
- [36] M. Nakamura, Phys. Rev. B **61**, 16377 (2000).
- [37] P. Sengupta, A. W. Sandvik, and D. K. Campbell, Phys. Rev. B **65**, 155113 (2002).
- [38] K. M. Tam, S. W. Tsai, and D. K. Campbell, Phys. Rev. Lett. **96**, 036408 (2006).
- [39] N. R. Cooper and G. V. Shlyapnikov, Phys. Rev. Lett. **103**, 155302 (2009).
- [40] A. J. Alexander, Phys. Chem. Chem. Phys. **7**, 3693 (2005).
- [41] T. U. Ito, W. Higemoto, K. Ninomiya, and H. S. Suzuk, Phys. Rev. B **84**, 064411 (2011).
- [42] J. M. Blatt and V. F. Weisskopf, *Theoretical Nuclear Physics* (Springer, 1979).
- [43] C. Bambi, Phys. Rev. D **83**, 103003 (2011).
- [44] M. R. Flannery, D. Vranceanu, and V. N. Ostrovsky, J. Phys. B **38**, S279 (2005).
- [45] M. Saffman, T. G. Walker, and K. Mølmer, Rev. Mod. Phys. **82**, 2313 (2010).
- [46] J. Polchinski, Nucl. Phys. B **231**, 269 (1984).
- [47] In contrast to a dipole which is analogous to a single-headed arrow ( $\uparrow$ ) pointing in a particular direction, a quadrupole corresponds to a double-headed arrow ( $\updownarrow$ ) not favoring one direction over another, and therefore it can be aligned, but not oriented.
- [48] Note the difference with dipole moments which can be nonzero only for states of indefinite parity (superposition of odd and even  $J$ 's)
- [49] Details on the FRG approach are provided in the supplemental online material.